ELSEVIER

Journal of Chromatography B, 743 (2000) 41–56

JOURNAL OF CHROMATOGRAPHY B

www.elsevier.com/locate/chromb

Analysis of brush-particle interactions using self-consistent-field theory

B.M. Steels, J. Koska, C.A. Haynes*

Biotechnology Laboratory, Department of Chemical and Bioresource Engineering and the Protein Engineering Network of Centers of Excellence, The University of British Columbia, 237 Wesbrook Building, Vancouver V6T 1Z3, Canada

Abstract

Non-specific protein adsorption can be reduced by attaching polymer chains by one end to a sorbent surface. End-grafted polymer modified surfaces have also found application in size-based chromatographic bioseparations. To better understand how to tailor surfaces for these applications, a numerical SCF model has been used to calculate theoretical results for the polymer density distribution of interacting polymer chains around a solute particle positioned at a fixed distance from a surface. In addition, the excess energy required to move the particle into the polymer chains (interaction energy) is calculated using a statistical mechanical treatment of the lattice model. The effect of system variables such as particle size, chain length, surface density and Flory interaction parameters on density distributions and interaction energies is also studied. Calculations for the interaction of a solute particle with a surface covered by many polymer chains (a brush) show that the polymer segments will fill in behind the particle quite rapidly as it moves toward the surface. When there is no strong energetic attraction between the polymer and solute we predict that the interaction energy will be purely repulsive upon compression due to losses in conformational entropy of the polymer chains. Above a critical chain length, which depends upon particle size, a maximum in the force required to move the particle toward the surface is observed due to an engulfment of the particle as chains attempt to access the free volume behind the particle. If an attraction exists between the polymer and solute, such that a minimum in the interaction energy is seen, the optimum conditions for solute repulsion occur at the highest surface density attainable. Long chain length can lead to increased solute concentration within the polymer layer due to the fact that an increased number of favourable polymer–solute contacts are able to occur than with short chains at a similar entropic penalty.

Keywords: Self-consistent field theory; Brush–particle interactions

1. Introduction

Polymer chains attached by one end to an interface are called a ‘‘brush’’ when the attachment points are close enough together that the chains interact with one another. This term is derived from a physical picture of tightly packed, partially ordered chains extending away from a surface. This asymmetric packing geometry leads to interesting physical behavior, which has been exploited in a number of applications. Significant research has been done to investigate the effectiveness of end-grafted polymers at improving biocompatibility of surfaces [1–3]. More recently, our group has exploited polymer brushes in a new chromatography mode, which we call Entropic Interaction Chromatography (EIC), for separating a wide range of analytes, including proteins and nucleic acids. EIC is based on the ability of an end-grafted polymer to effect a rapid size-based separation of solute molecules due to differences in

*Corresponding author.

0378-4347/00/$ – see front matter
PII: S0378-4347(00)00206-1

the entropy change accompanying their penetration into the brush [4]. A review by Milner [5] gives other examples of brush applications, which include surfactants, miscibility agents for polymer blends and colloid stabilization. Here, we develop a molecular model which provides a detailed picture of brush-protein interactions and thus a molecular theory for understanding both brush-based biomaterials and EIC.

Several molecular-based models have been developed for analyzing brush distributions as a function of system conditions [6–9] and the interaction of brushes with planar surfaces or other brushes [10–13]. Few studies however, have focused on a small impenetrable particle (a protein molecule perhaps) interacting with, or moving into, polymer chains that are end-grafted to a surface. The goal of this work is to gain a better understanding of how a solute molecule interacts with end-grafted polymer chains (Fig. 1). We develop an exact self-consistent-field (SCF) model, which allows for chain splaying, to calculate the density distribution and thermodynamics of end-grafted polymer around a particle positioned at various distances from the grafting surface. Our model is based on the original SCF model for polymer adsorption developed by Scheutjens and Fleer [14–16] with an extension to model end-grafted chains [6] in a cylindrical lattice geometry [17,18].

Computer simulations are particularly useful for visualizing polymers in solution because the small molecular size scale (nm) and the fact that the polymer density is usually low make detailed information difficult to obtain from experiment. Modeling work on brush-particle interactions, which may be compared to our results, includes an empirical model developed by Joen et al. [19,20], a description based on analytical SCF theory by Subramanian et al. [21] and a molecular dynamics calculation of Murat and Grest [22] for a related system in which an atomic force microscope tip is brought in contact with a brush.

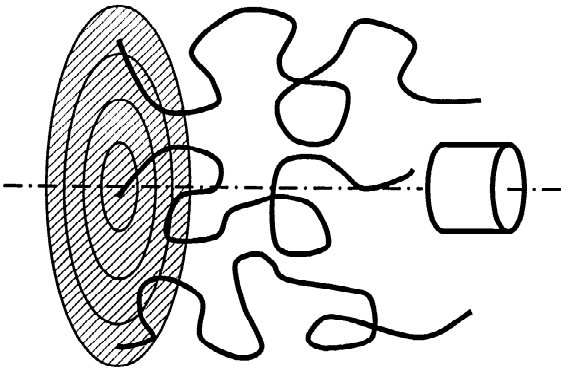

Fig. 1. Schematic diagram showing a solute molecule interacting with polymer chains end-grafted to a surface. The centerline represents the axis of a cylindrical coordinate system, and the rings on the surface represent spatial increments in the radial direction.

The semi-empirical model of Joen et al. represents the first attempt to analyze the interaction of a spherical solute with a brush, in this case end-grafted polyethylene oxide [19,20] (PEO). Interaction energies were calculated as the sum of a steric repulsion term, a van der Waals attraction term and a hydrophobic interaction term. The relatively simple model is based on an earlier scaling thermodynamic treatment of de Gennes and a critical assumption that the brush distribution assumes a step profile. Thus, the model assumes the brush is completely compressed with no splaying as the particle approaches. It predicts that solute repulsion increases with increasing particle penetration and with increasing chain length at a given chain density. It also predicts, somewhat surprisingly, that the optimum chain density for solute repulsion depends upon the particle size. For larger proteins with radius $R=60–80$ A, the optimum distance between grafting points d was found to be more than that for small proteins of radius $R=20$ A ($d=13–17$ A vs. 9–11 A).

Milner developed a more refined model for calculating brush distribution profiles using an analytical form of SCF theory. This result was extended by Subramanian et al. to evaluate the energy required to compress a brush with a cylinder. Like the earlier work of Joen et al., the resulting model is based on the untested, and possibly poor assumption that the grafted chains do not splay, and thus are completely compressed by the approaching particle.

Recently, Murat and Grest [22] report molecular dynamics (MD) simulation results for an AFM tip interacting with a brush, from which some insights for an interacting particle can be inferred. The simulations show that the applied force required increases with brush compression. However, the

increase in force is less than that predicted by the models of Joen et al. and Subramanian et al. because the MD simulations show that chain segments are able to escape from under the AFM tip. Larger tip sizes lead to a more rapid increase in compression force since it is more difficult for the chains to escape. However, since the chain segments are able to rearrange themselves around the tip, the segment density between the tip and the surface was found to remain approximately constant (the same as that of the undisturbed brush), in sharp contrast to predictions of the two earlier models.

The numerical self-consistent-field theory used in this work makes no a priori assumptions about the polymer chain configurations, or density distribution. Radials of lattice sites are treated with mean-field averaging, which is a reasonable assumption given the symmetry of the system when a cylindrical particle is moved toward the brush surface. By combining step-weighted walk statistics with equilibrium statistical thermodynamics we calculate the average density distribution of polymer segments in an undisturbed brush and around a particle. The energetic interaction (including entropic and enthalpic contributions) of the brush with the particle as it moves toward the grafting surface has been calculated and some potential applications for the model are explored.

2. Cylindrical mean-field lattice

Linear polymers are normally capable of adopting a very large number of conformations in solution since the bond rotation energy for a backbone C–C bond is on the same order of magnitude as the thermal energy of the system. By evaluating the number of possible ways in which the components of a constant energy system can be arranged Ω, it is possible to calculate statistical thermodynamic information (i.e. $S = -k \ln \Omega$). The counting of configurations for long polymer molecules is difficult, however, due to the enormous number of possible conformations the chains can adopt.

We have used a cylindrical lattice geometry developed by Leermakers et al. [17], in which rings of lattice sites are treated with mean-field averaging (Fig. 2), to compute average grafted-chain conformations and energetics. This geometry allows us to model a grafting surface at one end of the cylinder from which polymer chains extend into the solution in the z direction (normal to the surface). The undisturbed brush is completely uniform in the radial r direction. A particle, which is given a very high density ($\Phi_p \geq 0.99$) with a confined lattice volume, may then be specified at a position on the cylinder's axis at some distance z_p from the grafting surface. The most convenient geometry for the particle is that of a small cylinder with some radius R_p and length L_p. With mean-field variation in the radial direction, solution of the resulting SCF equations yields information about the radial and normal segment density distributions.

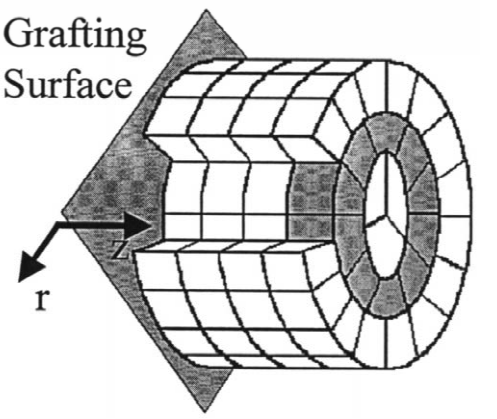

Fig. 2. Schematic diagram of the cylindrical lattice showing the coordinate directions z and r. The mean field applies to each radial $r(z)$ of the lattice as shown by the shaded radial.

We have followed the same geometry rules as Leermakers et al. [17], giving the cylindrical lattice flat layers numbered from $z = 1, \ldots, Z_{max}$ in the normal direction and rings numbered $r = 1, \ldots, R_{max}$ in the radial direction. The grafting surface is modeled as an impenetrable surface at position $z = 1$ (for all r), and all other surfaces ($z = Z_{max}$, $r = R_{max}$) are treated as reflecting boundaries. Boundary effects on the chains are made negligible by using a sufficiently large lattice. All lattice sites have equal volume, and the number of sites in a given radial r that is one layer thick is given by the area (in lattice units) of the radial:

$$L(r) = \pi[r^2 - (r-1)^2] \quad (1)$$

A ring's outer surface area is then given by:

$$S(r) = 2\pi r \tag{2}$$

In order to couple the different mean-field regions of the lattice together, we must calculate the probability to move from a given site to any adjacent site (perhaps in a different radial). These probabilities are a consequence of the lattice geometry, and are referred to as step probabilities λ. We will allow steps up (higher z), steps down or steps in the same layer while simultaneously allowing steps inward (lower r), steps outward or steps in the same radial shell.

In all calculations, we have assumed a hexagonal lattice (12 nearest neighbors) in which the probability to step up or down a layer is $\lambda_1(z) = \lambda_{-1}(z) = \frac{1}{4}$, and the probability to stay in the same layer is $\lambda_0(z) = \frac{1}{2}$. These probabilities correspond to the number of nearest neighbors in the adjacent layer or the same layer, respectively, divided by the total number of nearest neighbors. For radial steps inward or outward the probabilities are proportional to the lattice site surface area on the face that is crossed:

$$\lambda_{-1}(r) = \frac{S(r-1)}{L(r)} \times \frac{1}{4} \tag{3}$$

$$\lambda_0(r) = 1 - \lambda_{-1}(r) - \lambda_1(r)$$

$$\lambda_1(r) = \frac{S(r)}{L(r)} \times \frac{1}{4}$$

The probability for two independent events to occur simultaneously is the product of their individual probabilities. For a step down and outward simultaneously, the probability is thus

$$\lambda_{-1,1}(z,r) = \lambda_{-1}(z) \times \lambda_1(r) \tag{4}$$

and likewise for all other step directions.

3. Numerical self-consistent-field theory

The preference of a free segment of component i to be in a lattice site in radial (z,r) with respect to the bulk solution is given by a Boltzmann factor

$$G_i = \exp\left[\frac{-u_i(z,r)}{kT}\right] \tag{5}$$

which is commonly called the free segment weighting factor [14]. It represents the preference a free segment of component i has for being in radial (z, r) with respect to the bulk solution. The potential of mean force $u_i(z, r)$used to calculate the free segment weighting factor is given by the sum of an interaction potential u_i^{int} and a hard core potential u'. The interaction potential u_i^{int} is pair-wise additive and defines nonideal, nonoverlapping interactions between nearest neighbors. The hard core potential u' is independent of segment type and serves to adjust segment potentials to ensure that the lattice space is completely filled and no segment overlap occurs.

The interaction potential $u_i^{\text{int}}(z, r)$ is calculated using the local segment densities and interaction parameters χ_{ij} for unlike pair contacts:

$$\frac{u_i^{\text{int}}(z,r)}{kT} = \sum_j \chi_{ij}\left\{\langle \Phi_j(z,r)\rangle - \Phi_j^b\right\} \tag{6}$$

Here $\Phi_j(z, r)$ is the volume fraction of component j in radial (z, r). The volume fraction of a component in the bulk solution is denoted by the superscript b. The Flory–Huggins interaction parameter χ_{ij} represents the excess energy with respect to the unmixed components that is associated with one segment of i being completely surrounded by j (or vice versa). In Eq. (6), the summation on j may include the surface if an interaction between the surface and each component is specified. Because solution properties vary by radial, the (step-weighted) average volume fraction of j in contact with a site in radial (z, r) is required. This is denoted by the angular brackets and is given in expanded notation by

$$\langle \Phi_j(z,r)\rangle = \sum_{z'}\sum_{r'} \lambda_{z'-z,r'-r}(r,z)\Phi_j(z',r') \tag{7}$$

where the step probabilities give the fraction of the total possible site contacts that occur in each adjacent direction.

Combining the step probabilities with the free-segment weighting factors allows one to calculate the statistical weighting of any given conformation in the lattice with respect to chains in the bulk solution. The statistical weight of all possible conformations can be calculated using the recurrence relation

$$G_i(z, r, s+1|1) = G_i(z, r)\langle G_i(z, r, s|1)\rangle \tag{8}$$

where $G_i(z, r, s+1|1)$ is called the chain end weighting factor and gives the statistical weighting for a chain of $s+1$ segments to end in radial (z, r), after starting from an end segment with ranking 1. Again, the angular brackets represent a step-weighted nearest neighbor average $G_i(z, r)$ and is the free-segment weighting factor for a segment of type i in radial (z, r). The chain-end distribution function must be generated from each chain end (fixed and free) when modeling grafted chains, since inversion symmetry does not apply.

The restriction that all chains start at the surface is imposed by calculating the chain-end distribution functions from the following starting point:

$$G_i(z, r, s|1) = G_i(z, r); z = 1, \quad r = 1 \ldots R_{\max} \tag{9a}$$

$$G_i(z, r, s|1) = 0; z = 2 \ldots Z_{\max}, \quad r = 1 \ldots R_{\max} \tag{9b}$$

Eqs. (9a) and (9b) ''graft'' the chains to layer 1 of the cylinder. The complementary chain-end distribution function is then generated using Eq. (8) from the starting point $G_i(z, r, N|N) = G_i(z, r)$, where N is the number of segments in the chains, with no restrictions on the location of the free end.

The statistical weighting for inner chain segments can be calculated by coupling the chain-end weighting factors for shorter chains. By summing over all segment rankings s in the chain and then normalizing, the volume fraction of each component $\Phi_i(z, r)$ is calculated from:

$$\Phi_i(z,r) = C_i \sum_s \frac{G_i(z, r, s|1)G_i(z, r, s|N)}{G_i(z, r)} \tag{10}$$

where the factor $G_i(z,r)$ in the denominator eliminates double counting. The normalization constant C_i for chains fixed in the system (restricted equilibrium) is given by [17]

$$C_i = \frac{n_i}{\sum_z \sum_r L(r) G_i(z, r, N|1)} \tag{11}$$

where n_i is the number of molecules of component i in the lattice. C_i may be specified arbitrarily for all calculations in order to simulate different surface grafting densities.

Finally, the fractional surface coverage σ_i is calculated from n_i using

$$\sigma_i = \frac{n_i}{N_i A} \tag{12}$$

where A is the area of the grafting surface in lattice units squared. The fractional surface coverage gives the fraction of chains attached per surface site and may also be expressed as a percentage grafting density (i.e. $\sigma = 0.1 = 10\%$ surface coverage).

Three distinct segment types are specified in the model, including those of the brush (b), solvent (o) and particle (p). The solvent is in full equilibrium, and allowed to move in and out of the system under the constraint that the lattice remains filled. The brush is considered a uniform homopolymer, and the particle is assumed to have uniform properties, being composed of a fixed number of segments filling the geometry chosen for it.

Grafting can be simulated such that the chain segments attached at layer 1 redistribute themselves radially when a particle is placed very close to the surface, simulating what might occur if the graft were surface mobile, such as in a cell membrane. The chain ends can also be fixed ''covalently'' to the surface such that each grafted segment is confined to a specific radial at $z = 1$. In the latter case, the brush is fixed to the grafting surface by individually grafting chains to each radial. The number of chains used to calculate the normalization constant for each separate radial must then be calculated using the number of lattice sites in the radial and assuming a constant grafting density. The non-surface-mobile brush therefore consists of $R_{\max}$ components, for each of which Eq. (8) has a different starting point. Finally the total brush density distribution is calculated by summing the volume fractions of the separate components.

The equations described above constitute a set of self-consistent equations, which can be solved numerically using the method of Leermakers et al. [23]

4. Thermodynamics

Energies of interaction between a brush and a particle are calculated from the partition function of the system in a manner similar to that used in the

original SF model for polymer compression by a plate [13,24]. Here, the result varies to account for the radial non-uniformity of the cylindrical system. From statistical thermodynamics, the Helmholtz energy A is related to the canonical partition function Q by

$$A - A^* = -kT \ln(Q - Q^*) \tag{13}$$

where the asterisk represents the reference state, which we specify as components in the pure, amorphous, unmixed state.

It is possible to write the partition function in terms of its combinatorial Ω and energy U terms:

$$\ln\left(\frac{Q}{Q^*}\right) = \ln\left(\frac{\Omega}{\Omega^*}\right) - \left(\frac{U - U^*}{kT}\right) \tag{14}$$

In order to evaluate Q, both terms must be expressed using parameters available from the lattice model. The combinatorial term can be expressed in terms of the step probabilities and then corrected using a mean-field approximation to account for chain volume [16]. Expressing this as a sum over all component types in all possible conformations gives:

$$\ln\left(\frac{\Omega}{\Omega^*}\right) = \sum_z \sum_r \sum_i L(r) \Phi_i(z,r) \left\{ \frac{\ln \Phi_i^b}{N_i} + \ln G_i(z, r) \right\} \tag{15}$$

The energy term is based on nearest neighbor interactions described by the FH interaction parameter. The summation over all m components gives

$$\frac{(U - U^*)}{kT} = \sum_z \sum_r \sum_{i=1}^{m} L(r) \sum_{j=i+1}^{m} \Phi_i(z,r) \chi_{ij} \langle \Phi_j(z,r) \rangle \tag{16}$$

which is the total energy change associated with mixing the components in the lattice. Here, the number of lattice sites $L(r)$ multiplied by the volume fraction of i in radial (z,r) gives the number of segments of i in the radial.

Inserting Eqs. (14)–(16) into Eq. (13) gives our working expression for the Helmholtz energy:

$$\frac{(U - U^*)}{kT} = \sum_z \sum_r \sum_{i=1}^{m} L(r) \Phi_j(z, r) \left\{ \frac{\ln \Phi_i^b}{N_i} + \ln G_i(z,r) + \sum_{j=i+1}^{m} \chi_{ij} \langle \Phi_j(z, r) \rangle \right\} \tag{17}$$

In Eq. (17), the bulk volume fraction for the grafted components is zero, leading to an unbounded $\ln \Phi_i^b$ term [13]. To overcome this problem, we have replaced Φ_i^b for the grafted chains with a pseudo-equilibrium bulk volume fraction

$$\Phi_i^b = \frac{nN}{\sum_z \sum_r L(r) G_i(z, r, N|1)} \tag{18}$$

as suggested by Scheutjens and Fleer [24].

Solving Eq. (17) at two different particle positions allows calculation of the excess energy $A^{\text{int}}(z_p)$ associated with a brush-particle interaction [13]

$$A^{\text{int}}(z_p) = (A - A^*)(z_p) - (A - A^*)(\infty) \tag{19}$$

where the coordinate z_p represents the layer position of the leading edge of the particle. In our calculations, the particle is moved stepwise in the z-direction toward the surface. At each particle position the brush distribution and thermodynamics are calculated. The position $z_p = \infty$ gives the reference state where the particle has a negligible interaction with the brush.

5. Results and discussion

Self-consistent-field theory has been able to provide a fairly detailed description of brush profiles (in the absence of an interacting particle). Analytical SCF theory predicts that the brush will form a parabolic distribution away from a grafting surface in the limit of infinite chain length [8,25]. This is confirmed by neutron scattering data [26] and numerical SCF theory [6], which also predicts a slight depletion layer next to the surface and a tail region at the outer end of the brush for finite chain lengths under non-adsorbing conditions.

5.1. Segment–density distributions

Introduction of a particle changes the conformations of chains in a brush (Fig. 3). The distribution of chains of $N = 50$ segments at a grafting density of $\sigma = 0.1$ is shown in Fig. 3 for an interacting particle of radius $R_p = 3$ and length $L_p = 3$ (referred to as a 3 by 3 particle) at various distances from the surface. All results shown are for non-mobile brushes. Inter-

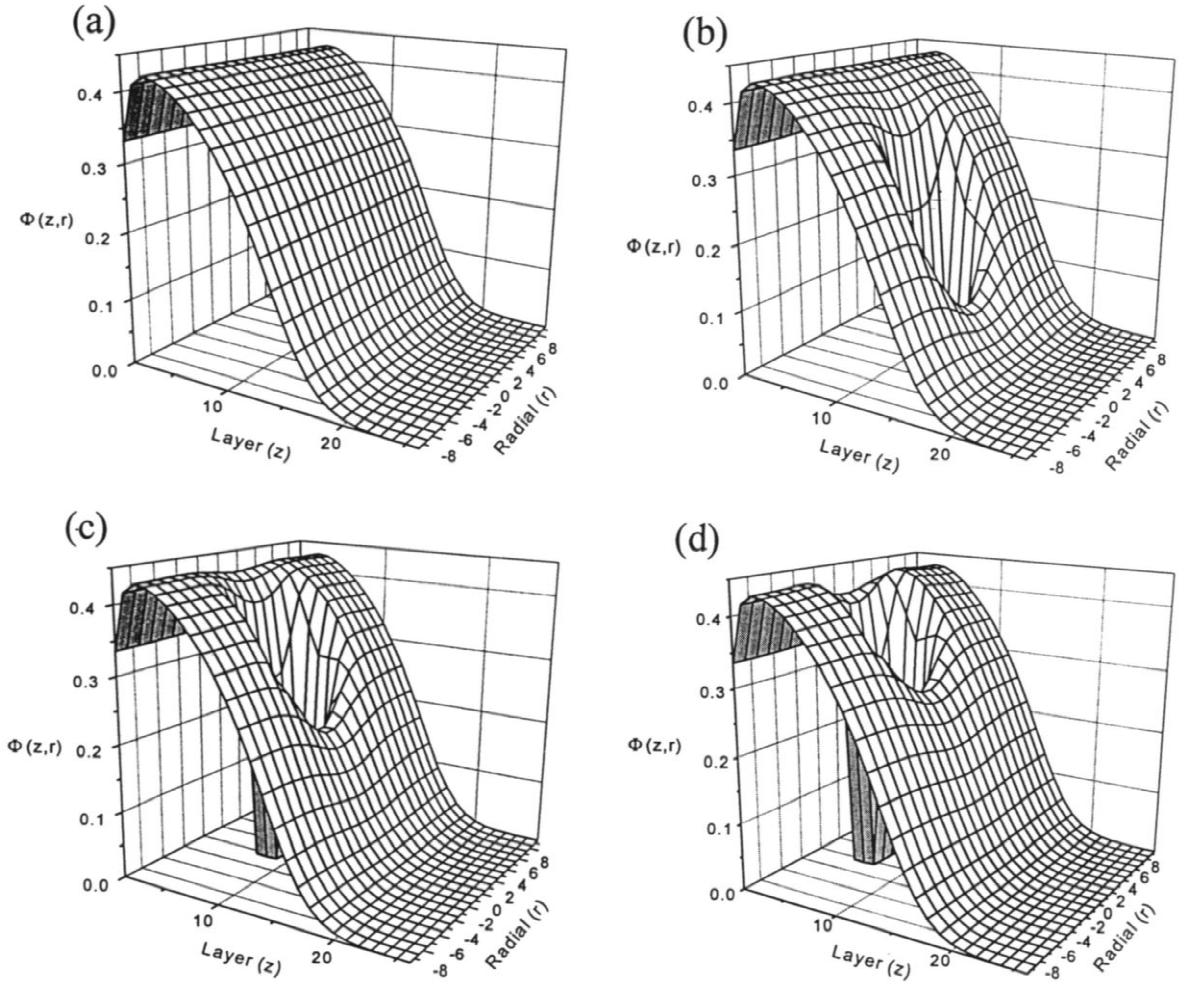

Fig. 3. Polymer segment density distributions in the cylindrical lattice are indexed in both the z and r directions. The chains of length $N=50$ with a grafting density of $\sigma=0.1$ are interacting with a particle of dimensions $R_p=3$ and $L_p=3$ (3 by 3). Interaction parameters are set as $\chi_{bo}=0.4$ and $\chi_{po}=0.4$ (unspecified interaction parameters are always zero). The density distribution is shown for a particle positioned (a) outside the brush, (b) at layer $z_p=10$, (c) $z_p=7$, and (d) $z_p=5$.

action parameters have been regressed from osmotic virial coefficients measured by Haynes et al. using low-angle laser-light scattering (LALLS) [27]. The interaction parameter for polyethylene glycol with water χ_{bo} lies between 0.45 and 0.5, depending on solution conditions. Interaction parameters for several proteins (lysozyme, bovine serum albumin, and α-chymotrypsinogen) with water χ_{po} lie in the range from 0.47 to 0.59, depending on protein size and net charge. Brush-particle interaction parameters χ_{bp}, estimated from cross-osmotic virial coefficients for protein/polymer pairs are all very close to zero [27]. Based on these results, we have set χ_{bo}, χ_{po}, and χ_{bp} to 0.4, 0.4 and 0, respectively, for most of our calculations. All other χ_{ij} were set to zero. In this way, the results should provide at least a qualitative picture of globular protein interactions with grafted PEG brushes, which are finding increased application as biomaterials and anti-fouling surfaces. In this context, it is worth noting that the calculated energy curves due to brush interaction with the particle are not very sensitive to the brush-solvent or particle–

solvent interaction parameters, but are sensitive to a favorable interaction between the brush and particle.

A brush density profile is shown in Fig. 3(a) at conditions where the particle is positioned outside the brush. The distribution is completely uniform in the radial direction, and shows a typical brush profile in the *z*-direction at near theta solvent conditions. The *z* and *r* coordinates on the plot index the mean-field radial of the cylinder, whose average brush segment volume fraction is shown on the vertical axis. A depletion layer is seen next to the grafting surface due to the entropic penalty the chains experience when steps are taken next to an impenetrable interface.

In Fig. 3(b–d), brush distributions are shown when the particle is sitting at layers $z_p = 10$, $z_p = 7$, and $z_p = 5$, respectively. For lattice sites occupied by the particle, the volume fraction of solvent and brush is essentially zero. As the particle begins to penetrate the brush, the segment density fills in quickly behind the particle, indicating chain splaying. To reach this extended chain state there is a concomitant depletion of the segment density between the particle and the surface (in front of the particle). Finally, when the particle reaches layer 5 (Fig. 3(d)), the segment density profile also increases slightly at the sides of the particle. This leads to a physical picture of grafted chains spread around the particle such that they radially partition away from the centerline, thereby lowering the brush density in the center of the particle's path.

Segment depletion between the particle and grafting surface does not occur at all conditions however. Fig. 4 shows the brush density distribution for four different chain lengths (at constant surface density), with a 3 by 3 particle sitting at layer 5. For a chain length of 15 segments (Fig. 4(a)) the segment density is enhanced slightly between the particle and the surface, indicating brush compression without significant chain splaying. Segment depletion is first observed at a chain length of $N = 25$ and becomes increasingly more pronounced with increasing chain length. Thus, the configuration of the grafted chains in the presence of a penetrating particle is a strong function of the chain length relative to the particle radius. This relationship has not been reported previously with modeling methods based on the Alexander–de Gennes brush [28,29] and analytical SCF theory [8], which do not allow splaying to occur.

Changing the surface density of the grafted chains also affects the density distribution of the brush. Fig. 5 shows a graft of $N = 50$ segment chains interacting with a 5 by 5 particle placed at layer 7. The chains are grafted at densities of $\sigma = 0.05$, $\sigma = 0.1$, $\sigma = 0.2$, and $\sigma = 0.3$ in Fig. 5(a–d), respectively. Increasing the surface density results in an extension of the brush and an increase in the segment–density maximum. At high surface densities, the brush profile begins to approach a step-profile in accordance with the Alexander–de Gennes brush model [28,29]. Unlike variations in chain length (see Fig. 4), increasing the grafting density does not in general lead to a transition from complete compression of the brush to a regime where chain splaying makes a dominant contribution to the perturbed density distribution. Instead, it changes the magnitude of segment compression or splaying. Changes in segment density in the region between the particle and the surface therefore become less significant with respect to the rest of the density profile.

5.2. Brush-particle interaction energies

The excess energy A^{int} required to move different sized particles into a brush is shown in Fig. 6. For a brush made up of 50-segment chains at a graft density of $\sigma = 0.1$, A^{int} increases with increasing particle size, particularly at deeper penetration depths. Under the chosen conditions, formation of contacts between brush and particle segments is enthalpically favorable since both segments have a net unfavorable interaction with the solvent ($\chi_{io} > 0$). Nevertheless, the calculated A^{int} values are always positive and increase sharply as the particle penetrates deeper into the brush. Thus, A^{int} is dominated by entropic effects, which are strongly repulsive due to the chain conformations that are eliminated by the presence of the particle. This result is the basis for entropic interaction chromatography, indicating that the (net repulsive) energy of interaction between particle and brush is a strong function of particle size. The strong entropic repulsion observed also shows that hydrophilic brushes should be effective in passivating a surface against adsorption of analytes

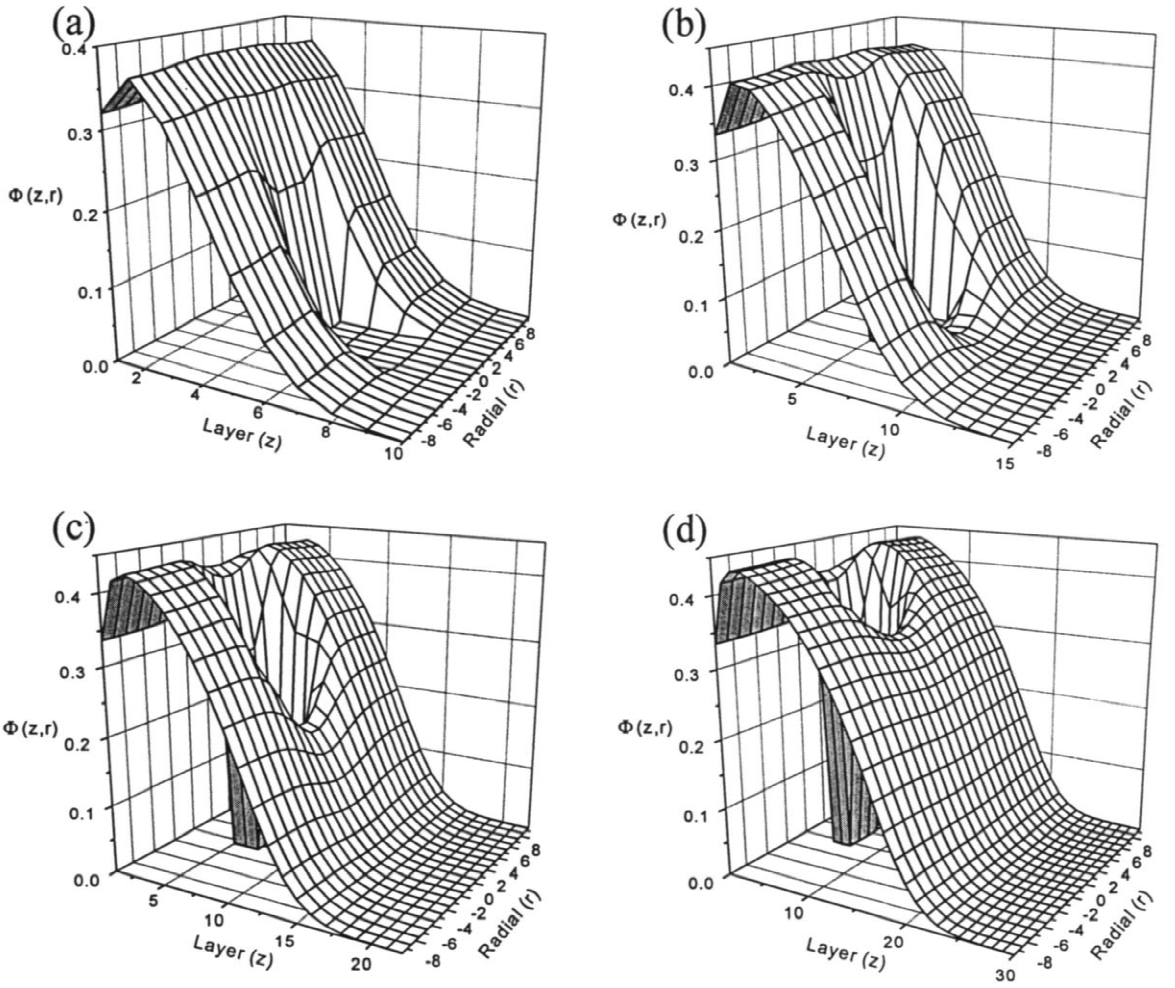

Fig. 4. Two-dimensional segment density distributions for four different chain lengths around a 3 by 3 particle placed with the leading edge at $z_p = 5$. Interaction parameters are specified as $\chi_{bo} = 0.4$ and $\chi_{po} = 0.4$. Chain lengths are (a) $N = 15$, (b) $N = 25$, (c) $N = 40$ and (d) $N = 60$ segments.

of almost any size, but particularly against large macromolecules such as proteins.

The effect of chain length on brush-particle interaction energies is shown in Fig. 7 for a 3 by 3 particle. As the chains are made longer the onset of an energetic repulsion occurs farther from the surface. This distance appears to scale linearly with N, as we might expect since brush height h also scales linearly with N [5]. For longer chains, A^{int} becomes nearly independent of chain length at particle positions close to the surface. This indicates that increased chain length allows chains to fill in the space behind the particle more easily. Once a particle has significantly penetrated a relatively long brush, the conformational entropy lost by the chains due to particle approach can be reduced by the gain of configurations of those chain segments which are able to step behind the particle.

The dotted lines in Figs. 6 and 7 intersect the energy curves at a point of inflection. Each inflection point represents a maximum in the force F required to move the particles into the brush, since $F = -\partial A^{int}/\partial z_p$. An inflection point is not observed for all combinations of N and R_p. Instead, there is a critical

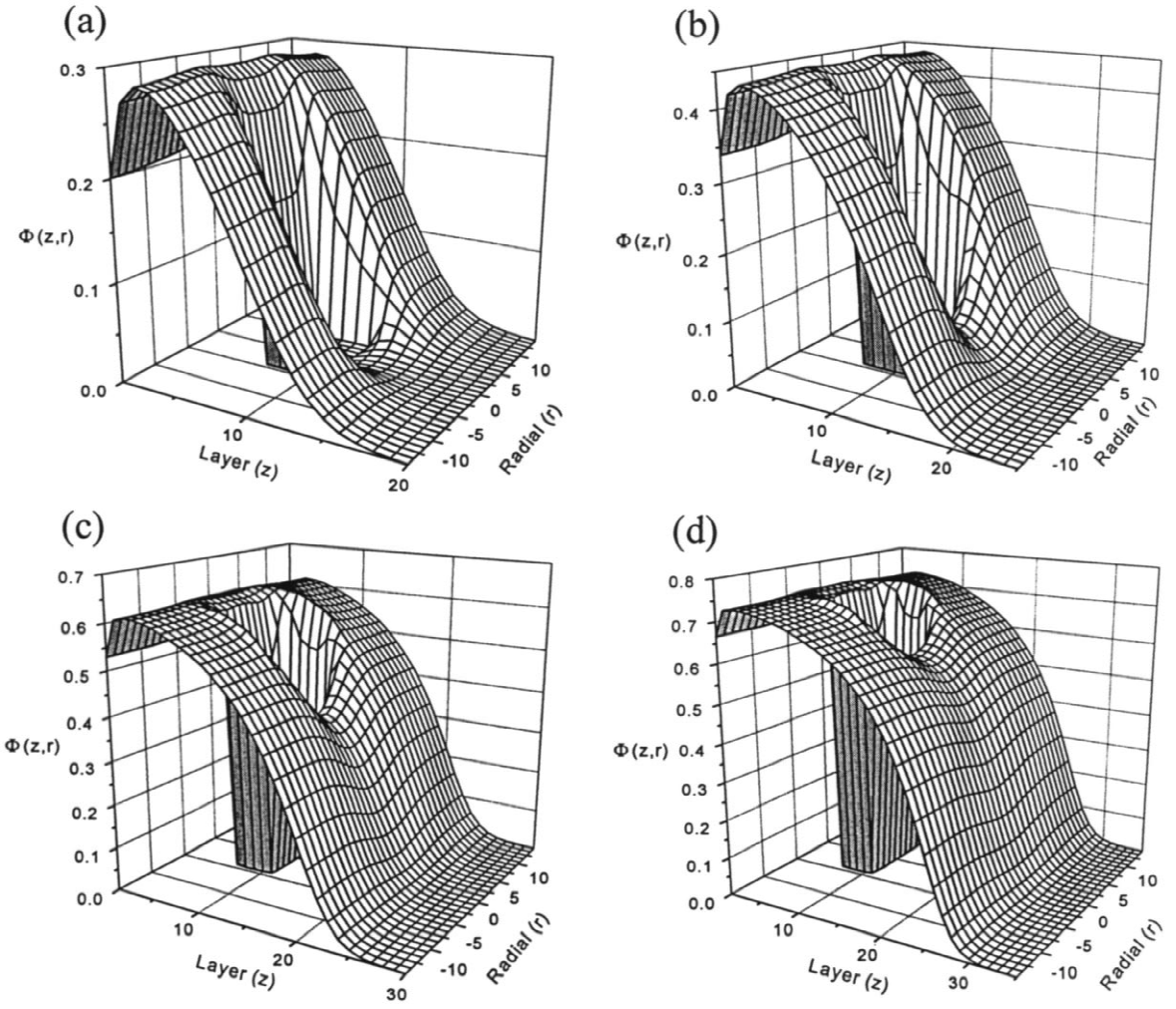

Fig. 5. Brush distribution of $N=50$ segment chains around a 5 by 5 particle at four different grafting densities. Interaction parameters are $\chi_{bo}=0.4$ and $\chi_{po}=0.4$. Grafting densities are (a) $\sigma=0.05$, (b) $\sigma=0.1$, (c) $\sigma=0.2$ and (d) $\sigma=0.3$.

chain length $N_{critical}$ above which an inflection point is seen for a given particle size. Fig. 8 shows $N_{critical}$ as a function of R_p for a constant grafting density of 10%. The critical chain length for this system increases linearly with R_p, in accordance with the increase in the distance that chain segments must extend in order to occupy space behind the particle. The minimum chain length for an inflection point in the limit of an infinitesimal particle is ca. 5 segments.

The change in brush-segment density profile which leads to the observed inflection point was analyzed by calculating A^{int} curves for penetration of a 3 by 3 particle under two limiting cases: (i) pure compression of the brush by the particle (which is equivalent to the model of Subramanian et al. [21]), and (ii) penetration into a brush in which all chains grafted directly beneath the particle have been removed (so that no chain splaying can occur).

Placing the boundary of the lattice in radial R_p+1, where R_p is the particle radius, allows the energy of pure chain compression to be calculated. Under this limiting condition, A^{int} increases monotonically with particle approach and no inflection point is observed.

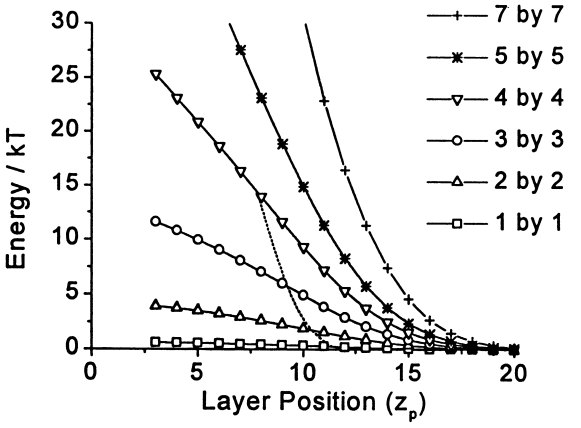

Fig. 6. Brush-particle interaction energy curves for chains of N=50 with a graft density of $\sigma=0.1$ interacting with various sized particles. Interaction parameters are specified as $\chi_{bo}=0.4$ and $\chi_{po}=0.4$. Particle size has been varied from $R_p=1$, $L_p=1$ up to $R_p=7$, $L_p=7$. The dashed line shows the inflection point of each such curve.

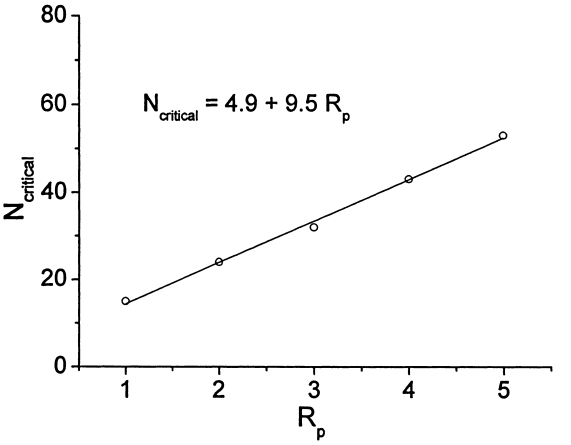

Fig. 8. The critical chain length $N_{critical}$ for which an inflection point is observed as a function of R_p for the system with $\sigma=0.1$; the interaction parameters are those in Fig. 7, and the particles have a cylindrical geometry where $L_p=R_p$.

Thus, the inflection point is related to chain segment escape from beneath the approaching particle. In principle, the inflection point could result from the lower energy of splayed chains relative to compressed chains and/or the increase in configurational entropy of chains which extend beyond the particle volume and can thereby step into the solvent-rich space behind the particle.

Results from limiting case (ii), where no chain splaying can occur, show an inflection point, suggesting that the inflection is due to the invasion of extended chain segments into the space behind the particle. As a result, A^{int} begins to decrease (indicating a slight attraction) as the particle is moved very close ($z_p<3$) to the grafting surface. Segment density profiles under this condition indicate that the chains adjacent to the side walls of the particle reach a lower energy state by stretching slightly in the z-direction to allow a larger number of segments to sample the volume directly behind the particle. A similar result, in which there is an inflection point and a decrease in A^{int} when the particle is close to the surface, is obtained when model calculations are carried out for a brush of surface-mobile chains. It is also worth noting that the model of Subramanian et al., which is limited by the severe assumption that chain splaying can not occur, does not predict the presence of an inflection point.

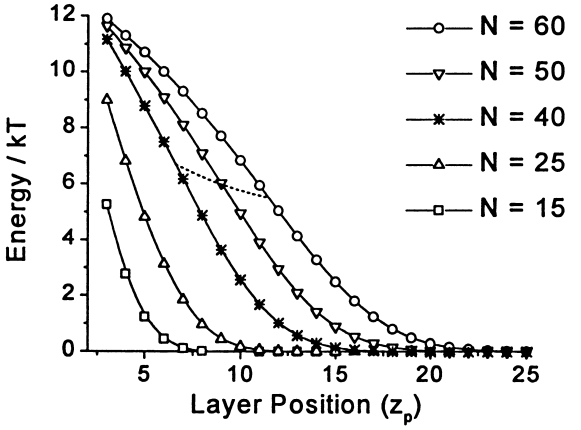

Fig. 7. Interaction energy curves for a particle of $R_p=3$, $L_p=3$ interacting with different length polymer chains of constant grafting density $\sigma=0.1$. Interaction parameters are $\chi_{bo}=0.4$ and $\chi_{po}=0.4$. The dashed line shows the inflection point of each curve.

As it penetrates the brush, a particle reduces the conformational entropy of the brush, increasing A^{int}. When the chains are able to gain a significant amount of conformational entropy by filling in behind the particle, the rate of increase in A^{int} with respect to particle position is reduced, giving rise to the observed inflection point. It is therefore useful to consider the segment density in the volume defined by the particle and the volume directly above and

below it. As the particle is moved toward the surface, the number of chain segments in the particle's path volume is always decreasing. As segments begin to fill in behind the particle, however, the rate of segment displacement changes. Fig. 9 shows the rate of decrease in the total number of segments (in front of and behind the particle) as a function of particle position; $-\partial A^{int}/\partial z_p$ is also shown for the same system. In systems where N is above $N_{critical}$, the inflection point in A^{int} always coincides with the point where the rate of displacement of segments by the particle is decreasing the fastest with respect to z_p. That is, where the rate of accumulation of segments behind the particle is a maximum.

The dependence of the inflection point position $z_{inflection}$ and the magnitude of the force maximum F_{max} on particle size, chain length and surface density were also investigated for specific cases. For a brush with $N=50$ and $\sigma=0.1$, the inflection point was found to move toward the surface in roughly linear proportion to R_p (Fig. 6). For the same system, F_{max} was found to increase in proportion to $R_p^{2.8}$, which suggests that it scales closely with particle volume. For a 3 by 3 particle and 10% grafting density (Fig. 7), $z_{inflection}$ moves away from the surface almost linearly with increasing N ($z_{inflection} \sim N^{0.8}$), which corresponds closely to the scaling of brush height. Furthermore, F_{max} was found to decrease with increasing chain length such that $F_{max} \sim N^{-1.2}$. Longer brush chains can more quickly adopt configurations that step behind a particle. This combined with the fact that a particle of fixed size will take away a smaller fraction of the conformations sampled by larger chains, results in an earlier inflection point in A^{int} and a lower F_{max}.

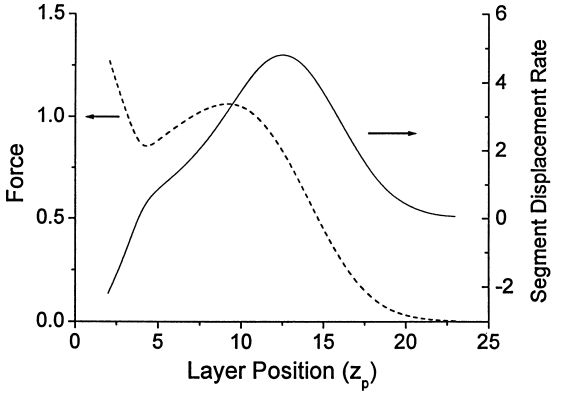

Fig. 9. The applied force F and the rate of segment displacement from the total volume the particle moves through as a function of z_p for a 3 by 3 particle moving into a brush with $N=50$ and $\sigma=0.1$.

5.3. Comparison with experiment

To confirm that our simulation results reflect true interaction energies between protein macromolecules and end-grafted polymer brushes, we have measured partition coefficients (Fig. 10) for a series of analytes ranging in size from glycerol (92.09 Da) to thyroglobulin (670 000 Da) on an acrylamide-based beaded (80 μm diameter) resin bearing a terminally attached brush of poly(methoxyethyl acrylamide) (PMEA). The Fractogel resin, kindly provided by E. Merck (Darmstadt, Germany), displayed a PMEA brush having a 3% surface grafting density and a

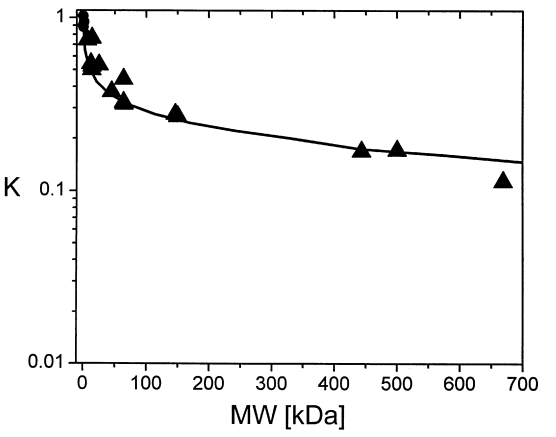

Fig. 10. Partition coefficient K data for a series of small analytes and globular proteins to the brush phase of BioSEC 656 Fractogel resin: total system volume=120.64 ml, resin packing density=0.443, resin porosity=0.76, surface grafting density=3%, SCF scaled chain DP=18±2, average bead diameter=80 mm, 50-m*M* phosphate buffer (pH 7) and 25°C. Analytes partitioned include glycerol (MW=92.09 Da), phenylalanine (115.13 Da), folic acid (441.4 Da), vitamin B12 (1355.4 Da), aprotinin (6500 Da), cytochrome c (12 327 Da), lactalbumin (14 200 Da), myoglobin (15 320 Da), chymotrypsinogen (26 500 Da), ovalbumin (45 000 Da), hemoglobin (64 500 Da), bovine serum albumin (66 000 Da), lactate dehydrogenase (140 000 Da), alcohol dehydrogenase (141 000 Da), apoferritin (443 000 Da), ferritin (502 000 Da), and thyroglobulin (670 000 Da). Solid curve: self-consistent field theory predictions with interaction parameters specified as $\chi_{bo}=0.4$, $\chi_{po}=0.4$ and $\chi_{pb}=0$.

scaled degree of polymerization between 16 and 20. The partition coefficient K_p is given by

$$K_p = \frac{C_p^{avg}}{C_p^{bulk}} = \frac{\int_{z=h}^{z_p=0} K_p(z_p)\, dz_p}{\int_{z=h}^{z_p=0} dz_p} \quad (20)$$

where C_p^{avg} and C_p^{bulk} are the average solute concentrations in the brush phase and the bulk liquid phase, respectively. Details of the partition coefficient measurement are given elsewhere [30].

In the ideal solution limit, the Boltzmann factor $K_p(z_p) = \exp(-A^{int}(z_p)/kT)$, gives the concentration of solute particles $C_p(z_p)$ at position z_p with respect to the bulk solution $C_p(z_p) = C_p^{bulk} \times K_p(z_p)$. The last equality in Eq. (20) therefore provides a method for predicting solute partition coefficients from calculated interaction energies such as shown in Fig. 7. In Eq. (20), h is the brush height arbitrarily chosen as the point at which the volume fraction of an undisturbed brush falls below 0.1%. Multiplying the average concentration by the height of the brush gives a value that is proportional to the number of particles that are interacting with the brush.

Comparison of the experimental data with the model predictions shows that the theory quantitatively captures the strongly nonlinear dependence of ln K_p on protein molecular weight (model scaling of protein MW values was based on protein radius of gyration data). Since we assumed in the model calculations that $\chi_{bp} = 0$, the observed exclusion effect, which increases strongly with increasing solute MW, is solely due to a loss of brush conformational entropy when the solute penetrates the brush volume. It is therefore a perfectly general effect that does not depend to any significant extent on specific chemical properties of the solute.

5.4. Adsorption on and in brushes

Fundamental modeling of protein adsorption on brush surfaces is severely limited. Joen et al. [19,20] have predicted a minimum in the interaction energy (negative A^{int}) between a protein and a polyethylene oxide brush surface when a strong hydrophobic interaction free energy term is included in their semi-empirical model. Penetration of the particle into the grafting surface, however, results in a strong steric repulsion that leads to a monotonically increasing interaction free energy. To better understand these effects, we have set the brush-solvent χ_{bo}, particle–solvent χ_{po}, and the brush-particle χ_{bp} interaction parameters in our model to 0.5, 0.5 and -0.5 respectively (all other $\chi_{ij} = 0$), which together define a strong enthalpic attraction between particle and brush segments.

The interaction energy for various sized particles with a 50-segment brush at 10% grafting density is shown in Fig. 11. When the particles interact with the surface of the brush, favorable brush-particle energetic contacts dominate the interaction energy, leading to negative values of A^{int}. With further penetration, a net energetic repulsion occurs once the loss of chain entropy is greater than the favorable contact energy, as predicted by Joen et al. [20]. As the particle size increases, the position of the onset of energetic repulsion z_{onset} occurs sooner (higher z_p). As shown in Fig. 11, the increase in z_{onset} with particle size gets progressively smaller as the particle size becomes larger. Eventually, z_{onset} reaches a constant value, equal to that for compression by an infinite flat plate.

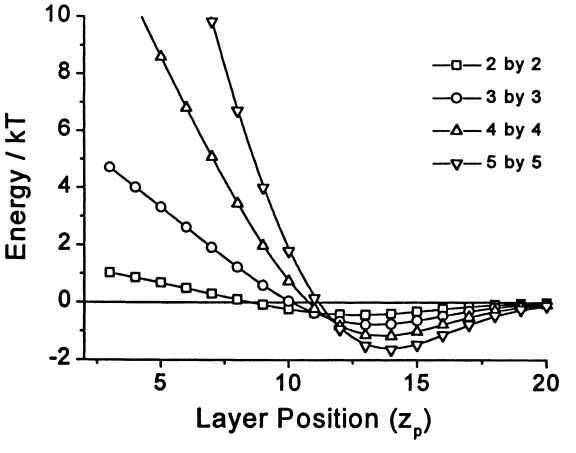

Fig. 11. Brush-particle interaction energy curves for four different sized particles interacting with chains of length $N = 50$ and grafting density $\sigma = 0.1$. Interaction parameters are $\chi_{bo} = 0.5$, $\chi_{po} = 0.5$ and $\chi_{bp} = -0.5$.

As the particle size increases, the magnitude of the attractive minimum $|A^{int}_{min}|$ increases significantly such that $|A^{int}_{min}| \sim R_p^{1.8}$. Thus, $|A^{int}_{min}|$ scales closely with particle surface area, which in turn scales with the number of contacts that brush and solvent segments make with the surface of the particle. The minimum in A^{int} indicates that the solute particles can preferentially adsorb to the surface of a brush under appropriate conditions.

It is important to note that a strongly negative brush-particle interaction parameter ($\chi_{bp} = -0.5$) is required to see a minimum in A^{int} with our model. The magnitude of χ_{bp} in this case is almost unrealistic for an interaction that is not electrostatic in nature, suggesting that perhaps Joen et al. might have over-estimated the hydrophobic interaction energy favoring adsorption. Experiments on brushes of short PEG chains show that a small amount of protein adsorption can be observed [31,32], suggesting a weak net attraction between polymer and protein. Interaction parameters calculated from data of Haynes et al. [27] also show that the polymer–protein interaction is weak in these systems, with a maximum attractive value of ca. $\chi_{bp} = -0.1$.

The dependence of A^{int}on σ is shown in Fig. 12. The brush consists of 50 segment chains that are interacting with a 5 by 5 particle. As the grafting density is increased, Z_{onset} increases with increasing $\sigma(Z_{onset} \sim \sigma^{0.4})$ due to the extension of the brush with increased graft density. The model also predicts that A^{int}_{min} decreases slightly with increasing σ and is shifted away from the grafting surface. The gradual increase in the attractive minimum results from more brush-particle contacts at higher surface density. However, the entropic repulsion scales more strongly with increasing σ than the energetic attraction, and as a result the attractive regions of the A^{int} curves become narrower with increasing σ. These two effects agree with the observation that a brush profile becomes more step-like as surface density is increased. The dependence of A^{int}_{min} on σ is quite weak, however, and the scaling therefore difficult to determine.

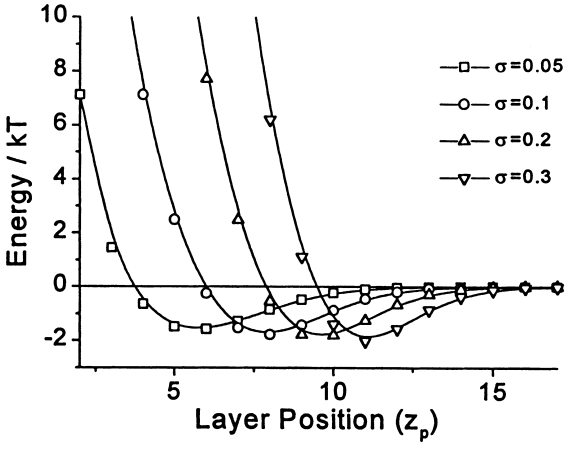

Fig. 12. Brush-particle interaction energy curves for a 5 by 5 particle penetrating chains of length $N=25$ at four different grafting densities. Interaction parameters are $\chi_{bo}=0.5$, $\chi_{po}=0.5$ and $\chi_{bp}=-0.5$.

Finally, we have investigated the effect of N on the interaction energy for this set of interaction parameters (not shown). z_{onset} shifts away from the surface approximately linearly with increasing N, again corresponding to the extension of the brush from the surface. The minimum in A^{int} becomes slightly shallower with increasing N, although the dependence appears very weak. However, longer chains have a broader attractive minimum than short chains. This may be because long chains are able to form multiple contacts with the particle over a wider range of particle positions.

5.5. Model application to the engineering of biomaterials

If the criterion for protection of a surface is the distance at which a repulsion energy begins, z_{onset}, then for a given brush length and surface density we predict that larger particles should be repelled better. Also, because h and z_{onset} increase with increasing N and σ, maximum repulsion will be obtained with long chains at the highest surface density possible.

The magnitude and width of the attractive minimum may also be important considerations if it is necessary to minimize any possible interaction between a protein and the brush. For example, studies have shown that although grafted polymer will strongly inhibit platelet adhesion, transient contacts can still lead to platelet activation and decreased platelet counts [33]. An alternate criteria for choosing the optimum surface coverage may therefore be to maximize z_{onset} while at the same time minimizing

the concentration of particles in the region of attractive interaction with the brush. Predicting the optimum conditions then becomes more difficult.

According to the Boltzmann factor (see Eq. (18)), the region of negative interaction energy will have a higher concentration of particles than in the bulk solution, while the repulsive region has a much lower concentration. In order to determine optimum brush conditions when considering both the magnitude and width of the minimum, it is useful to calculate the average concentration of solute particles in the brush. We predict that the total number of particles interacting with the brush decreases with increasing σ due to the narrower attractive region at higher σ (Fig. 12). Therefore, increasing surface density for a given chain length should always improve resistance to solute interaction with a surface, even in cases where brush-particle attraction occurs.

When chain length is increased, the width of the attractive minimum is increased causing an increase in partitioning of particles to the brush surface region. This suggests that very long flexible chains may actually be less effective at reducing adsorption, especially since experimentally, lower surface densities are normally obtained with higher degrees of polymerization. Under conditions of weak attraction, the optimum properties of end-grafted polymer for protection against adsorption are therefore a combination of low N and high σ that gives an acceptable value of z_{onset}.

It is important to note that we find a different result for optimum protein repulsion than Joen et al. [19,20]. Their steric repulsion term, based on an energy balance between a chain stretching term and an osmotic energy term, does not allow the brush to splay around the protein. We have shown that splaying is an important phenomenon in the case where a small to moderate-sized particle penetrates a brush. Their model assumes a constant density for the brush, which increases as the protein moves toward the surface. As a result, they overestimate the density of polymer between the particle and the surface and thereby predict very large repulsive energies. Moreover, by adding a steric repulsion term to a hydrophobic interaction energy term, they have assumed that the terms are thermodynamically additive. This is almost certainly a poor assumption, since entropy plays a significant role in the steric repulsion by the polymer chains as well as in the hydrophobic interaction energy.

Other work which considers the mechanism of protein repulsion by polymers such as PEG predicts that it may be due to the hydrophilic nature of the polymer, or the strong hydration shell required to solvate the polymer [34]. Our calculations suggest that while those may contribute, the dominant effect in protein repulsion is the high degree of flexibility in the polymer chains, which in thermodynamic terms is seen as high conformational entropy. Penetration of a particle into the chains decreases the chain entropy, giving rise to a sharp increase in the brush-particle interaction energy. This is supported by the results of Schroën et al. [35] who found that an extended brush configuration of adsorbed Pluronic copolymer was significantly better at reducing protein adsorption than a collapsed layer, even though the surface was made more hydrophilic in both cases.

Acknowledgements

This work was supported in part by a Strategic Grant from the Natural Science and Engineering Research Council of Canada (NSERC), an NSERC graduate fellowship (BMS), and the Protein Engineering Network of Centers of Excellence. The authors are particularly grateful to Dr. Frans Leermakers for assistance in model development.

References

[1] C.H. Bamford, K.G. Al-Lamee, Clin. Mater. 10 (1992) 243–261.
[2] D.L. Elbert, J.A. Hubbell, Annu. Rev. Mater. Sci. 26 (1996) 365–394.
[3] M.C. Woodle, D.D. Lasic, Biochim. Biophys. Acta 1113 (1992) 171–199.
[4] D. Brooks, V.J. Muller, Molecular Recog. 9 (1996) 697–700.
[5] S.T. Milner, Science 251 (1991) 905–914.
[6] T. Cosgrove, T. Heath, Macromolecules 20 (1987) 1692–1696.
[7] P-G. de Gennes, Macromolecules 13 (1980) 1069–1075.
[8] S.T. Milner, T.S. Witten, M.E. Cates, Macromolecules 21 (1988) 2610–2619.
[9] M. Murat, G. Grest, Macromolecules 22 (1989) 4054–4059.

[10] J.I. Martin, Z.-G. Wang, J. Phys. Chem. 99 (1995) 2833–2844.
[11] E. Ruckenstein, B.Q. Li, J. Chem. Phys. 107 (1997) 932–942.
[12] M. Murat, G.S. Grest, in: R.J. Roe (Ed.), Computer Simulation of Polymers, Prentice Hall, Englewood Cliffs, N.J, 1993, pp. 141–153.
[13] B. Van Lent, R. Israels, J.M.H.M. Scheutjens, G.J.J. Fleer, Colloid Interface Sci. 137 (1990) 380–394.
[14] J.M.H.M. Scheutjens, G.J.J. Fleer, Phys. Chem. 83 (1979) 1619–1635.
[15] J.M.H.M. Scheutjens, G.J.J. Fleer, Phys. Chem. 84 (1980) 178–190.
[16] G.J. Fleer, M.A. Cohen Stuart, J.M.H.M. Scheutjens, T Cosgrove, B. Vincent, Polymers at Interfaces, Chapman & Hall, London, 1993.
[17] F.A.M. Leermakers, J.M.H.M. Scheutjens, J. Lyklema, Biochim. Biophys. Acta 1024 (1990) 139–151.
[18] B.M. Steels, C.A. Haynes, F.A.M. Leermakers, Analysis of Compression of Polymer Mushrooms using Self-Consistent Field Theory, submitted to J. Chromatogr. A, 1999.
[19] S.I. Jeon, J.D.J. Andrade, Colloid Interface Sci. 142 (1991) 159–166.
[20] S.I. Jeon, J.H. Lee, J.D. Andrade, P.-G. de Gennes, J. Colloid Interface Sci. 142 (1991) 149–158.
[21] G. Subramanian, D.R.M. Williams, P.A. Pincus, Macromolecules 29 (1996) 4045–4050.
[22] M. Murat, G.S. Grest, Macromolecules 29 (1996) 8282–8284.
[23] F.A.M. Leermakers, J.M.H.M. Scheutjens, J. Chem. Phys. 89 (1988) 3264–3274.
[24] J.M.H.M. Scheutjens, G.J. Fleer, Macromolecules 18 (1985) 1882–1900.
[25] C.M. Wijmans, J.M.H.M. Scheutjens, E.B. Zhulina, Macromolecules 25 (1992) 2657–2665.
[26] T. Cosgrove, K. Ryan, Langmuir 6 (1990) 136–142.
[27] C.A. Haynes, F.J. Benitez, H.W. Blanch, J.M. Prausnitz, AIChE Journal 39 (1993) 1539–1557.
[28] S.J. Alexander, Phys. (Paris) 38 (1977) 977–987.
[29] P.G.J. de Gennes, Phys. (Paris) 37 (1976) 1443–1452.
[30] D.E. Brooks, C.A. Haynes, D. Hritcu, B.M. Steels, W. Muller, Proc. Nat. Acad. Sci. (USA), accepted, 2000.
[31] A. Kishida, K. Mishima, E. Corretge, H. Konishi, Y. Ikada, Biomaterials 13 (1992) 113–118.
[32] E.W. Merril, Poly(ethylene glycol) chemistry, in: J.M. Harris (Ed.), Biotechnical and Biomedical Applications, Plenum Press, New York, 1992, pp. 199–220.
[33] G.R. Llanos, M.V.J. Sefton, Biomedical Materials Res. 27 (1993) 1383–1391.
[34] G.C. Gölander, J.N. Herron, K. Lim, P. Claesson, P. Stenius, J.D. Andrade, Poly(ethylene glycol) chemistry, in: J.M. Harris (Ed.), Biotechnical and Biomedical Applications, Plenum Press, New York, 1992, pp. 221–245.
[35] C.G.P.H. Schroen, M.A.C. Stuart, K.V. Maarschalk, A. Vanderpadt, K. Vantriet, Langmuir 11 (1995) 3068–3074.